Supplementary Material

Graphene oxide coated functional separators as efficient metal chlorides blocking layers for chloride ion batteries

Chang Zhang[a,d], Shijiao Sun[a,d*], Kan-Hao Xue[b], Yingchun Miao[c], Xiulan Hu[a,d*], Xiangyu Zhao[a,d*]

[a] State Key Laboratory of Materials-Oriented Chemical Engineering, College of Materials Science and Engineering, Nanjing Tech University, 30 Puzhu South Road, Nanjing 211816, China

[b] School of Integrated Circuits, Huazhong University of Science and Technology, Wuhan 430074, China

[c] Advanced Analysis and Testing Center, Nanjing Forestry University, Nanjing 210037, China

[d] Jiangsu Collaborative Innovation Center for Advanced Inorganic Functional Composites, Nanjing Tech University, 30 Puzhu South Road, Nanjing 211816, China

Corresponding authors:

Email address:

sunshijiao@njtech.edu.cn; whoxiulan@163.com; xiangyu.zhao@njtech.edu.cn

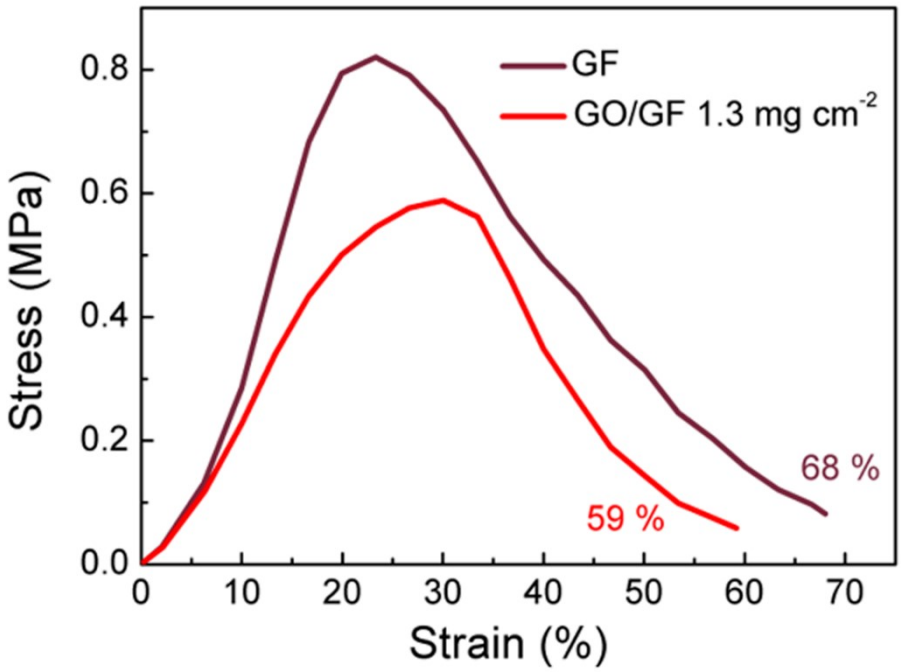

Fig. S1. Stress-strain curves of the pristine GF separator and the GO/GF 1.3 mg cm^{-2} separator.

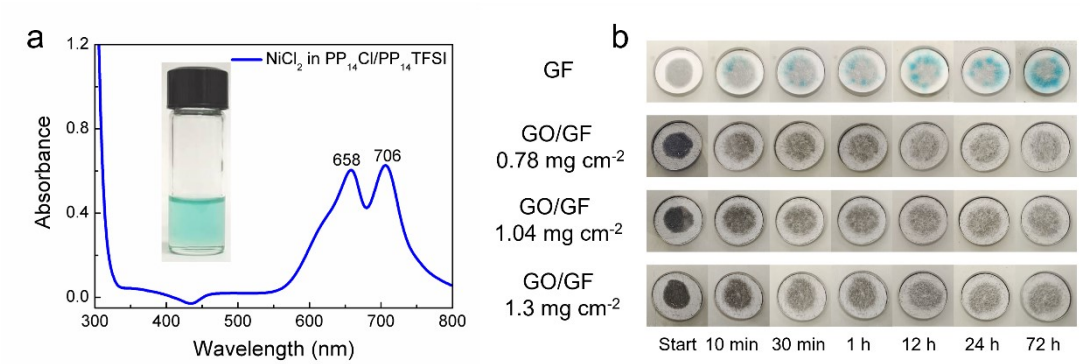

Fig. S2. (a and inset) UV-Vis spectra and photographs of the $NiCl_2$ dissolved in $PP_{14}Cl/PP_{14}TFSI$ electrolyte. (b) Diffusion test of the $NiCl_2$ cathode containing the pristine GF separator and the GO/GF separators with different loading contents.

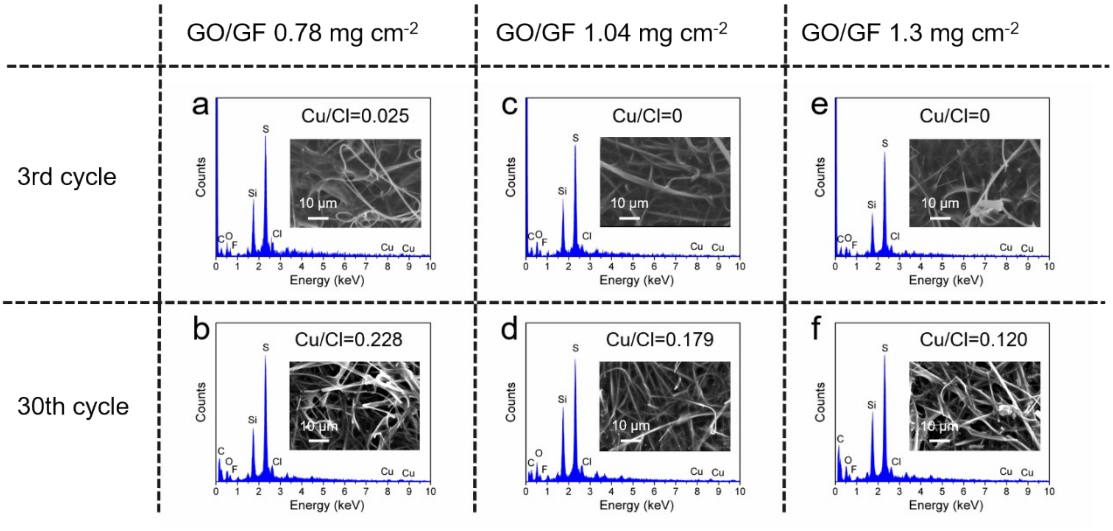

Fig. S3. FE-SEM images and the corresponding EDS patterns of the GO/GF separators with different loading contents for the $CuCl_2$ cathode after 3 and 30 cycles.

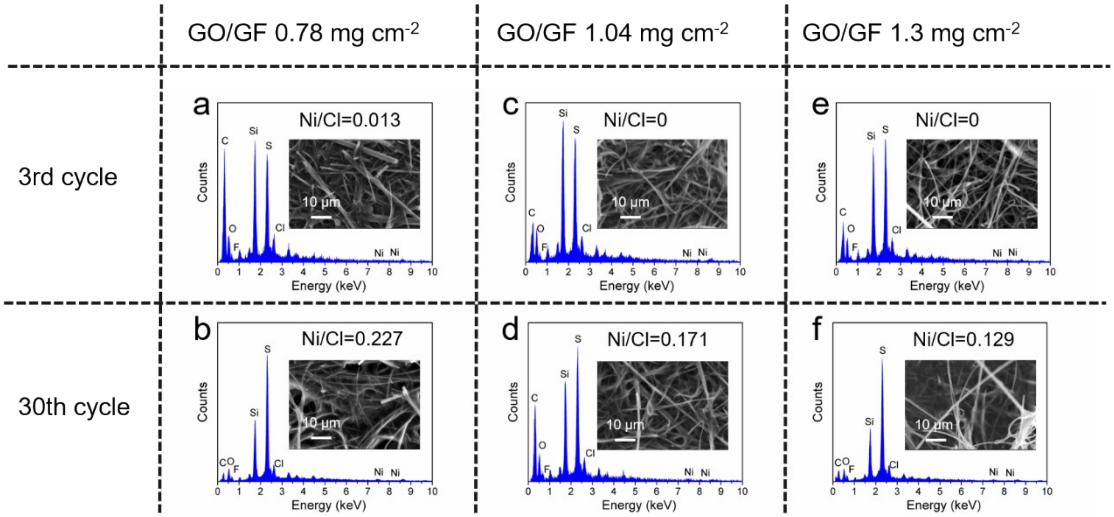

Fig. S4. FE-SEM images and the corresponding EDS patterns of the GO/GF separators with different loading contents for the $NiCl_2$ cathode after 3 and 30 cycles.

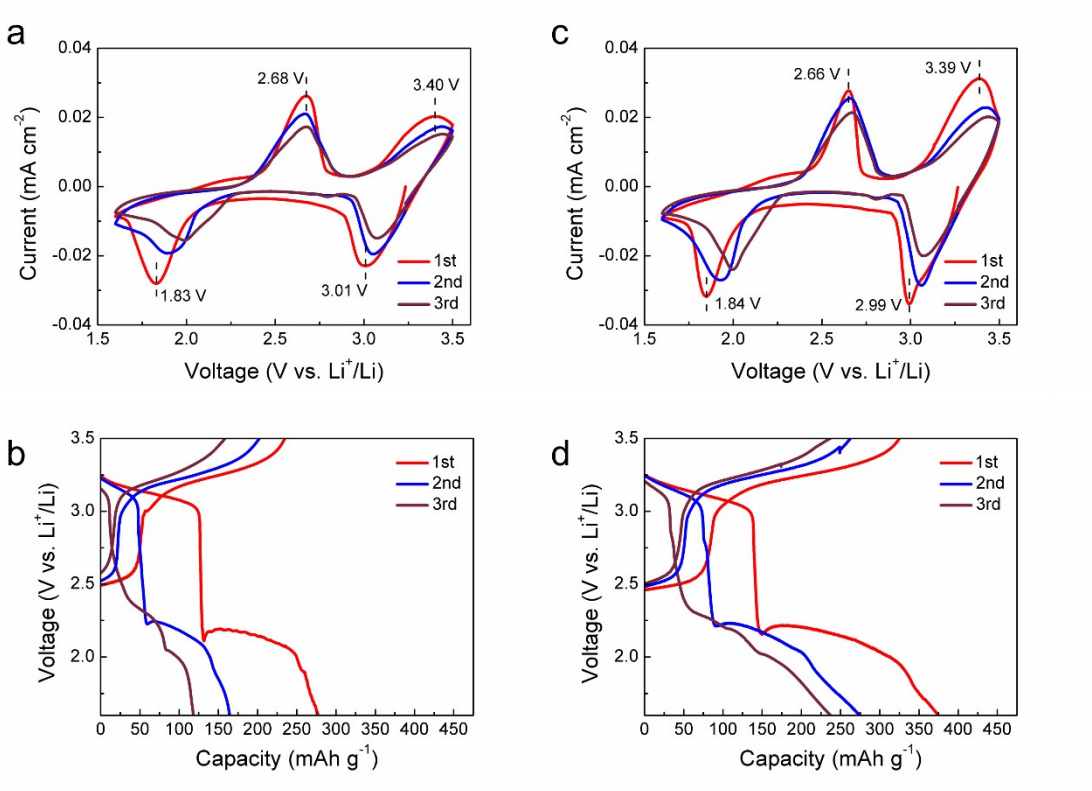

Fig. S5. CV curves and discharge-charge curves of the $CuCl_2$ cathode with (a, b) the GO/GF 0.78 mg cm^{-2} separator and (c, d) the GO/GF 1.04 mg cm^{-2} separator.

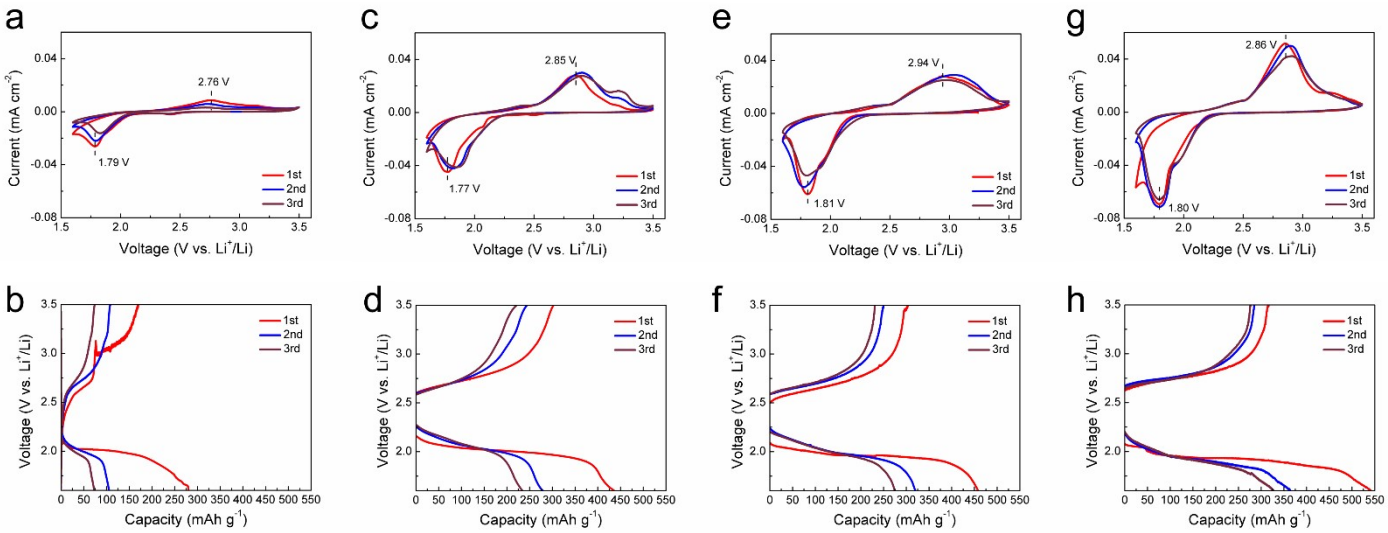

Fig. S6. CV curves and discharge-charge curves of the $NiCl_2$ cathode with (a, b) the pristine GF separator, (c, d) the GO/GF 0.78 mg cm^{-2} separator, (e, f) the GO/GF 1.04 mg cm^{-2} separator, and (g, h) the GO/GF 1.3 mg cm^{-2} separator.

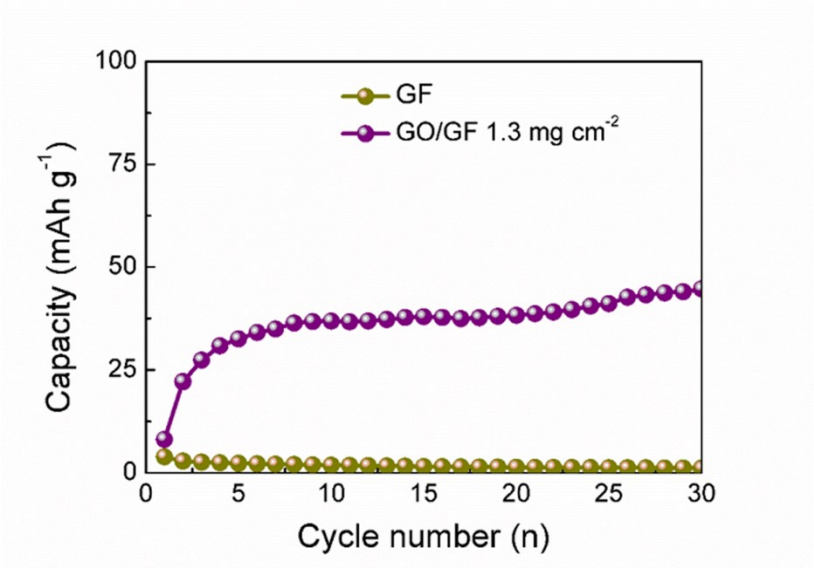

Fig. S7. Cycling performance of blank cathode with the pristine GF separator and the GO/GF 1.3 mg cm^{-2} separator.

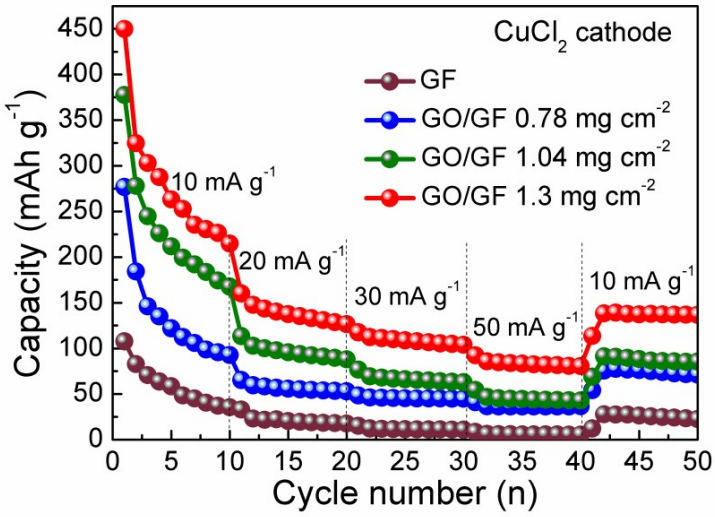

Fig. S8. Rate performance of the cells containing the pristine GF separator and the GO/GF separators with different loading contents for the $CuCl_2$ cathode.

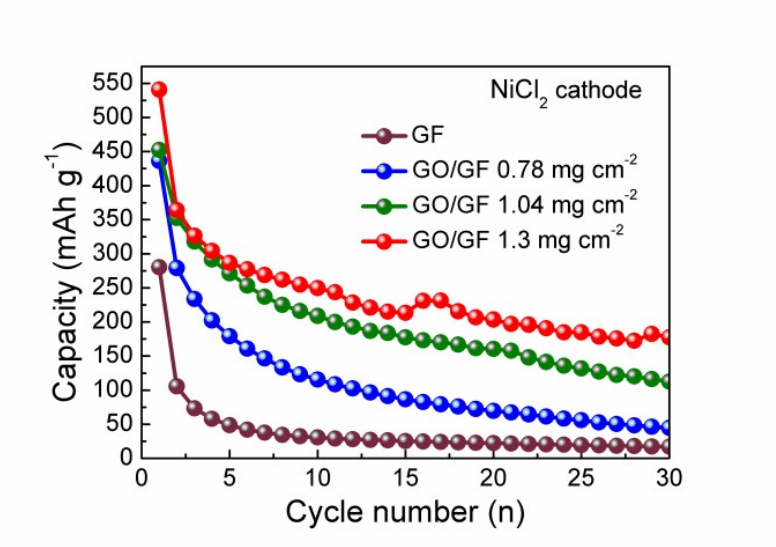

Fig. S9. The cycling performance of the cells containing the pristine GF separator and the GO/GF separators with different loading contents for the $NiCl_2$ cathode at 10 mA g^{-1} (0.024C).

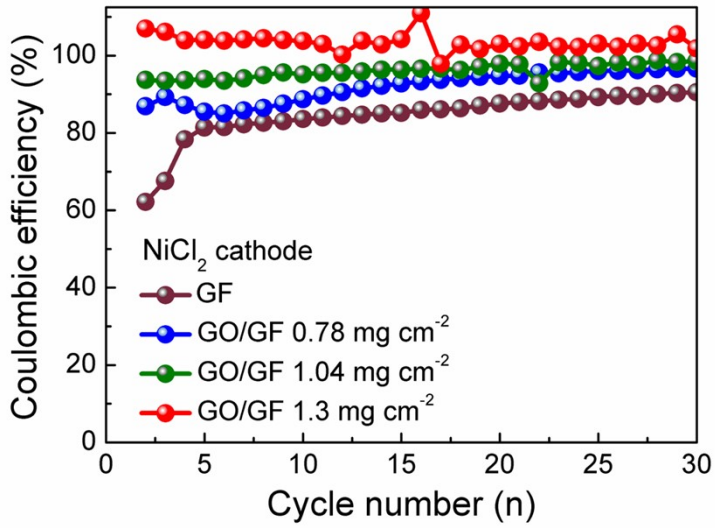

Fig. S10. The Coulombic efficiency of the cells containing the pristine GF separator and the GO/GF separator with different loading content during cyclic test at 10 mA g^{-1} for the $NiCl_2$ cathode.

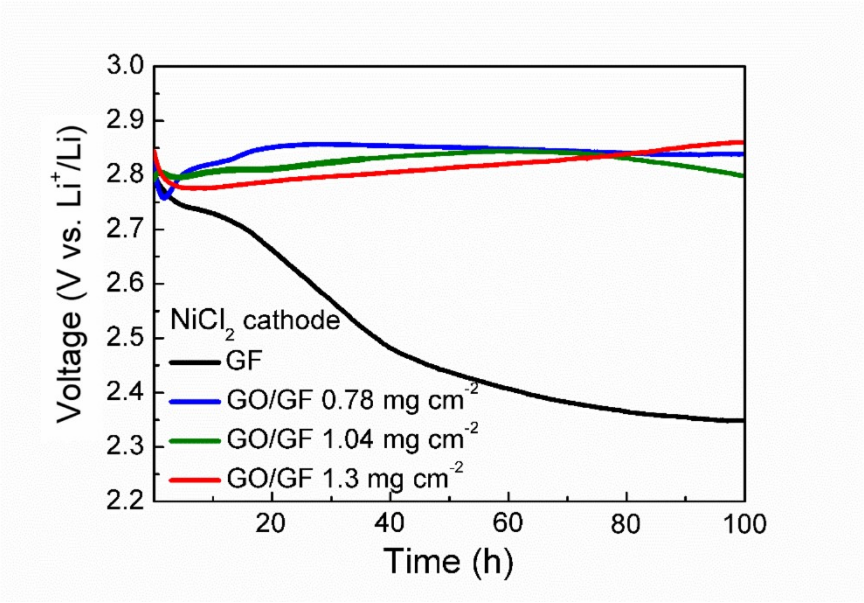

Fig. S11. The open circuit voltage profiles of the cells containing the pristine GF separator and the GO/GF separators with different loading contents for the $NiCl_2$ cathode.

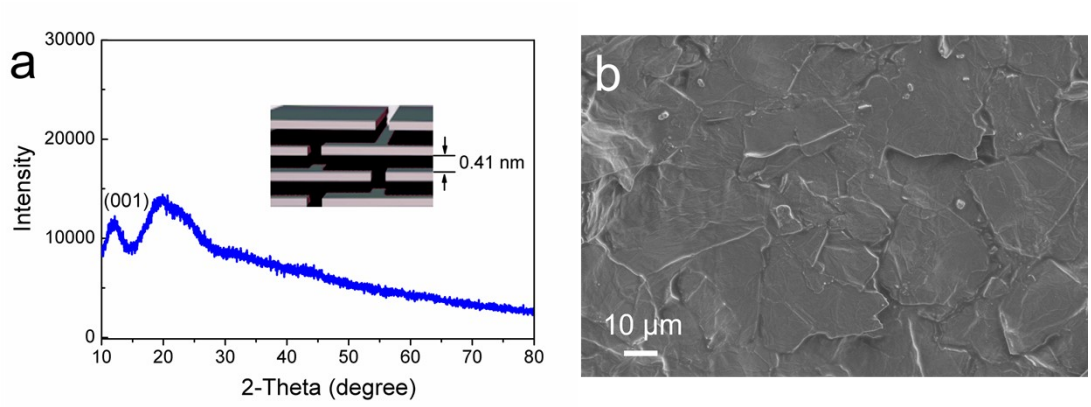

Fig. S12. (a) Wide-angle XRD pattern and (b) FE-SEM image of the GO/GF 1.3 mg cm^{-2} separator after 30 cycles.

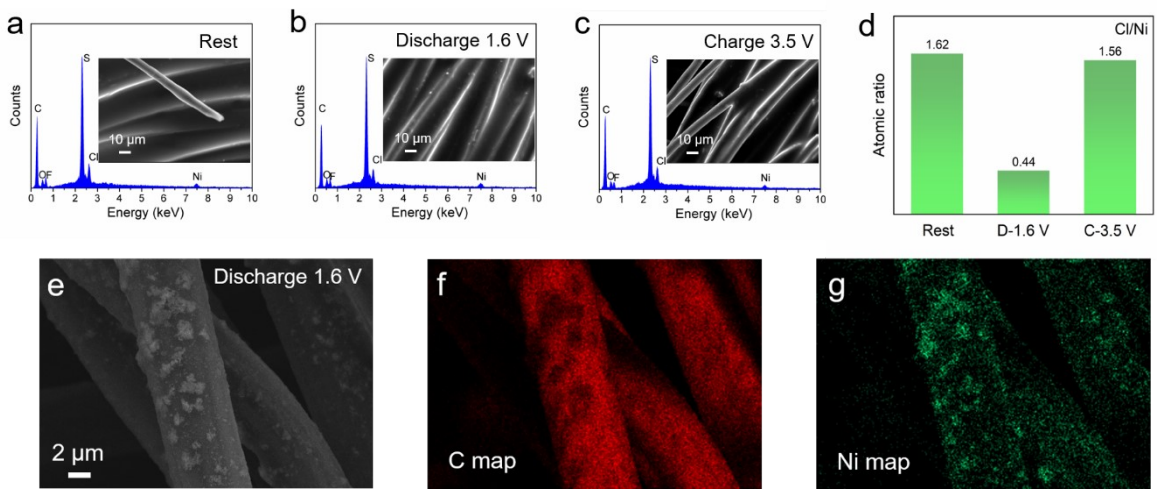

Fig. S13. (a-c) FE-SEM images and corresponding EDS spectra of the $NiCl_2$ cathode at various electrochemical states during the first cycle. (d) Atomic ratio of Cl and Ni elements. (e-g) Elemental mapping of the cathode at the fully discharged state.

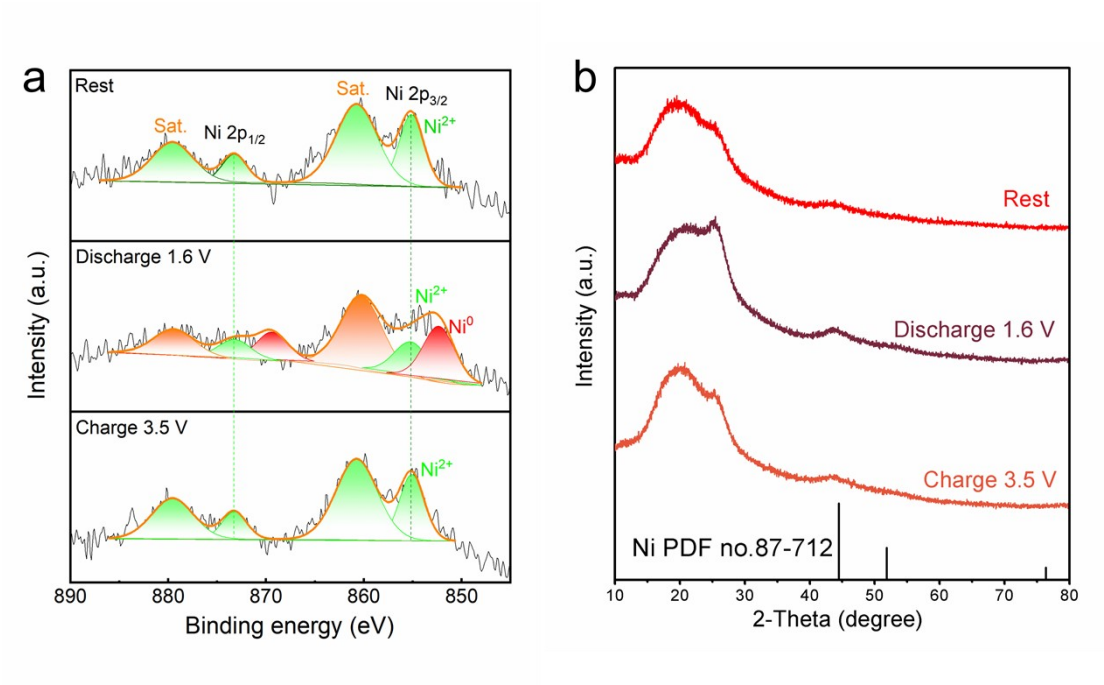

Fig. S14. (a) Ex-situ XRD patterns and (b) XPS spectra of the $NiCl_2$ cathode at various electrochemical states during the first cycle.

Table S1. Electrochemical data of metal chloride cathodes for CIBs.

Cathode	n	Calculated voltage (vs. Li^+/Li)[a]	Theoretical specific capacity		Theoretical energy density	
		V	Ah kg^{-1}	Ah L^{-1}	Wh kg^{-1}	Wh L^{-1}
VCl_3	3	2.22	511.2	1475.8	1133.8	3273.4
$CrCl_3$	3	2.31	507.7	1476.4	1170.2	3403.1
$MnCl_2$	2	1.70	425.9	1272.6	724.5	2164.7
$FeCl_3$	3	2.80	495.7	1443.5	1389.4	4046.1
$CoCl_2$	2	2.59	412.8	1408.5	1067.5	3642.3
$NiCl_2$	2	2.64	413.6	1460.4	1092.7	3858.4
$CuCl_2$	2	3.07	398.7	1353.2	1225.6	4159.7
$ZnCl_2$	2	2.07	393.3	1179.5	814.1	2441.6
$GaCl_3$	3	2.41	456.6	1127.8	1101.8	2721.4
$ZrCl_4$	4	1.68	460.0	1288.0	771.9	2161.3
$NbCl_5$	5	2.57	496.0	1383.8	1273.7	3553.7
$MoCl_5$	5	3.11	490.5	1398.4	1524.0	4344.9
$SnCl_2$	2	2.50	282.7	1252.9	707.0	3133.6
WCl_6	6	3.20	405.5	1427.4	1296.0	4561.8
$BiCl_3$	3	2.90	255.0	1211.3	738.5	3507.8

[a]The voltage is calculated by the thermodynamic equation: $\Delta G = -nEF$, where the Gibbs free energy data come from the literature entitled "Standard thermodynamic properties of chemical substances".

Table S2. Electrochemical performance data of our $CuCl_2$, $NiCl_2$ cathodes and other previously reported cathodes of metal chlorides, metal oxychlorides, organic substances containing chlorine, layered double hydroxides and MXene for CIBs at ambient temperature.

Cathode	Electrolyte	Mass loading (mg cm^{-2})	Current density (mA g^{-1})	Median discharge voltage (V)	Maximum discharge capacity (mAh g^{-1})	Cycle life (n)	Gravimetric energy density (Wh Kg^{-1})	Ref.
$CoCl_2$	[OMIM]Cl in [BMIM]BF_4	/	1 mA g^{-1} (0.002C)	2.5	64	1	160	[1]
VCl_3	[OMIM]Cl in [BMIM]BF_4	/	1 mA g^{-1} (0.002C)	2.4	90	1	215	[1]
$BiCl_3$	[OMIM]Cl in [BMIM]BF_4	/	3 mA g^{-1} (0.012C)	2.4	114	3	274	[1]
$BiCl_3$@MCF	$PP_{14}Cl$ in $PP_{14}TFSI$	1.5	10 mA g^{-1} (0.039C)	2.4	199	60	478	[2]
FeOCl	$PP_{14}Cl$ in $PP_{14}TFSI$	/	10 mA g^{-1} (0.04C)	2.1	126	30	265	[3]
BiOCl	$N_{116(14)}Cl$ in $N_{1114}TFSI$	/	5 mA g^{-1} (0.049C)	2.19	48	6	105	[3]
VOCl	$PP_{14}Cl$ in PC	/	2C	1.4	106	50	148	[4]
FeOCl/graphene	$PP_{14}Cl$ in $PP_{14}TFSI$	/	10 mA g^{-1} (0.04C)	2.24	118	6	264	[5]
FeOCl/CMK-3	$PP_{14}Cl$ in $PP_{14}TFSI$	/	10 mA g^{-1} (0.04C)	2.18	105	30	229	[6]

FeOCl@Pani	$PP_{14}Cl$ in $PP_{14}TFSI$	/	10 mA g^{-1} (0.04C)	1.95	87	50	170	[7]
FeOCl@PPy	$PP_{14}Cl$ in $PP_{14}TFSI$	1.4	10 mA g^{-1} (0.04C)	2.12	101	30	214	[8]
$Sb_4O_5Cl_2$-GAG	$PP_{14}Cl$ in PC	1.5–2	10 mA g^{-1} (0.12C)	1.3	183	80	238	[9]
$WOCl_4$	$Pyr_{14}Cl$ in PC&EC	2	C/10	1.29	96	50	124	[10]
FeOCl@MCF	$PP_{14}Cl$ in $PP_{14}TFSI$	1.5	10 mA g^{-1} (0.04C)	2.24	85	30	190	[11]
$PPyCl_{0.33}$@CNTs	$PP_{14}Cl$ in $PP_{14}TFSI$	3.5–4.5	10 mA g^{-1} (0.087C)	2.33	77	40	179	[12]
PANI/CNTs	$PP_{14}Cl$ in $PP_{14}TFSI$	/	10 mA g^{-1} (0.16C)	2.32	29	50	68	[13]
$PXVCl_2$/G	$PP_{14}Cl$ in PC	/	10 mA g^{-1} (0.061C)	2	95	60	190	[14]
Ni(dpip)	$BPy_{14}Cl$ in PC	1.5	150 mA g^{-1}	1.68	105	200	176	[15]
CoFe-Cl LDH	$Bpy_{14}Cl$ in $PP_{14}TFSI$&PC	1–1.5	100 mA g^{-1} (1.62C)	1.49	143	100	214	[16]
NiFe-Cl LDH	$BPy_{14}Cl$ in PC	1.5	100 mA g^{-1} (1.25C)	1.57	246	800	386	[17]
CoNi-Cl LDH	$BPy_{14}Cl$ in PC	1–1.5	100 mA g^{-1} (1.25C)	1.63	112	50	183	[18]

NiMn-Cl LDH/CNT	$BPy_{14}Cl$ in PC	1–1.5	50 mA g^{-1}	1.6	180	150	287	[19]
$Ni_2V_{0.9}Al_{0.1}$-Cl LDH	$Bpy_{14}Cl$ in $PP_{14}TFSI$&PC	1–1.5	100 mA g^{-1} (0.81C)	1.66	207	1000	344	[20]
Ni_5Ti-Cl LDH	$BPy_{14}Cl$ in PC	1.3	300 mA g^{-1} (4.7C)	1.57	159	1000	250	[21]
$Mo_{0.3}NiCo_2Cl$ LDH	$BPy_{14}Cl$ in PC	1.2	150 mA g^{-1} (0.34C)	1.57	182	300	286	[22]
$Ti_3C_2Cl_2$	$Bpy_{14}Cl$ in $PP_{14}TFSI$&PC	1	200 mA g^{-1}	0.54	375	1000	203	[23]
$CuCl_2$	$PP_{14}Cl$ in $PP_{14}TFSI$	0.57	10 mA g^{-1} (0.025C)	2.45	452	30	1107	This work
$NiCl_2$	$PP_{14}Cl$ in $PP_{14}TFSI$	0.57	10 mA g^{-1} (0.024C)	1.89	541	30	1022	

Supplementary Note 1. First-principles calculation

There is no unique criterion to fix the size of an ion, therefore we have carried out first-principles calculations to evaluate the sizes of $[CuCl_4]^{2-}$ and $[NiCl_4]^{2-}$ on an equal footing. The strategy is to optimize the structure of these composite anions so as to find the pairs of ions that are most far apart. The distance between them is denoted by L. Subsequently, the Shannon ionic radii of both ions are further considered. Hence, the diameter of the composite anion D is defined as

$$D = L + R_1 + R_2$$

where R_1 and R_2 are the Shannon ionic radii of the two relevant ions, respectively. We carried out density functional calculations using the Vienna *Ab initio* Simulation Package (VASP) with the projector augmented-wave method. The plane wave basis was cut off at a 500 eV kinetic energy. The exchange-correlation functional was selected as the Perdew-Burke-Ernzerhof form of generalized gradient approximation (GGA). The valence electrons were set as: 3d and 4s for Cu; 3d and 4s for Ni; 3s and 3p for Cl. In each case, a $2 \times 2 \times 2$ nm^3 periodic box was used to contain the composite anion, and two more electrons were added per box to account for the actual charge status. The optimized composite anions are as follows, in VASP POSCAR format.

$[CuCl_4]^{2-}$

```
CuCl4
1.0
20.0000000000000000    0.0000000000000000    0.0000000000000000
 0.0000000000000000   20.0000000000000000    0.0000000000000000
 0.0000000000000000    0.0000000000000000   20.0000000000000000
Cl    Cu
4      1
Direct
0.5000000000000000  0.5000000000000000  0.3845078302636232
0.5961666365637701  0.5586655266016357  0.5244452100662353
0.3925424686321427  0.5345670677232934  0.5237120960489891
0.5105637180832646  0.4068304237713690  0.5671358375645220
0.5000000000000000  0.5000000000000000  0.5000000000000000
```

$[NiCl_4]^{2-}$

```
NiCl4
1.0
20.0000000000000000    0.0000000000000000    0.0000000000000000
 0.0000000000000000   20.0000000000000000    0.0000000000000000
 0.0000000000000000    0.0000000000000000   20.0000000000000000
Cl    Ni
4      1
Direct
0.5000000000000000  0.5000000000000000  0.3845134942903933
0.5920314597209677  0.5608979906465492  0.5337570759015192
0.4036235837399210  0.5446645934254516  0.5476056033959363
0.5000000000000000  0.5000000000000000  0.5000000000000000
0.5153118137918783  0.3907164195632516  0.5334323703555272
```

[1] X.Y. Zhao, S.H. Ren, M. Bruns and M. Fichtner, *J. Power Sources*, 2014, **245**, 706-711.

[2] C. Zhang, S.J. Sun, M.F. Wu and X.Y. Zhao, *Chin. Chem. Lett.*, 2022, **33**, 2200-2204.

[3] X.Y. Zhao, Z.R. Zhao-Karger, D. Wang and M. Fichtner, *Angew. Chem. Int. Ed.*, 2013, **52**, 13621-13624.

[4] P. Gao, M.A. Reddy, X.K. Mu, T. Diemant, L. Zhang, Z.R. Zhao-Karger, V.S.K. Chakravadhanula, O. Clemens, R.J. Behm and M. Fichtner, *Angew. Chem. Int. Ed.*, 2016, **55**, 4285-4290.

[5] X.Y. Zhao, Q. Li, T.T. Yu, M. Yang, K. Fink and X.D. Shen, *Sci. Rep.*, 2016, **6**, 19448.

[6] T.T. Yu, Q. Li, X.Y. Zhao, H. Xia, L.Q. Ma, J.L. Wang, Y.S. Meng and X.D. Shen, *ACS Energy Lett.*, 2017, **2**, 2341-2348.

[7] T.T. Yu, R.J. Yang, X.Y. Zhao and X.D. Shen, *ChemElectroChem*, 2019, **6**, 1761-1767.

[8] R.J. Yang, T.T. Yu and X.Y. Zhao, *J. Alloys Compd.*, 2019, **788**, 407-412.

[9] Q. Zhang, R. Karthick, X.L. Zhao, L.G. Zhang, Y.M. Shi, L.F. Sun, C.Y. Su and F.M. Chen, *Nanoscale*, 2020, **12**, 12268-12274.

[10] G. Karkera, M. Soans, B. Dasari, E. Umeshbabu, M.A. Cambaz, Z. Meng, T. Diemant and M. Fichtner, *Energy Technol.*, 2022, **10**, 2200193.

[11] C. Zhang, S.J. Sun, M.F. Wu and X.Y. Zhao, *ACS Appl. Mater. Interfaces*, 2023, **4**, 5209-5217.

[12] X.Y. Zhao, Z.G. Zhao, M. Yang, H. Xia, T.T. Yu and X.D. Shen, *ACS Appl. Mater. Interfaces*, 2017, **9**, 2535-2540.

[13] Z.G. Zhao, T.T. Yu, Y.C. Miao and X.Y. Zhao, *Electrochim. Acta*, 2018, **270**, 30-36.

[14] T.C. Xia, T.T. Zhu, Y.C. Miao and X.Y. Zhao, *ACS Appl. Energy Mater.*, 2022, **5**, 6980-6985.

[15] Q. Yin, Z.H. Song, S.H. Yang, G.D. Wang, Y.W. Sui, J.Q. Qi, D.Y. Zhao, L. Hou, and Y.Z. Li, *Chem. Sci.*, 2023, **14**, 5643-5649.

[16] Q. Yin, D.M. Rao, G.J. Zhang, Y.J. Zhao, J.B. Han, K. Lin, L.R. Zheng, J. Zhang, J.S. Zhou and M. Wei, *Adv. Funct. Mater.*, 2019, **29**, 1900983.

[17] Q. Yin, J.N. Luo, J. Zhang, L.R. Zheng, G.Q. Cui, J.B. Han and D. O'Hare, *J. Mater. Chem. A*, 2020, **8**, 12548-12555.

[18] Q. Yin, J. Zhang, J.N. Luo, J.B. Han, M.F. Shao and M. Wei, *Chem. Eng. J.*, 2020, **389**, 124376.

[19] J.N. Luo, Q. Yin, J. Zhang, S.X. Zhang, L.R. Zheng and J.B. Han, *ACS Appl. Energy Mater.*, 2020, **3**, 4559-4568.

[20] Q. Yin, J.N. Luo, J. Zhang, S.X. Zhang, J.B. Han, Y.J. Lin, J.S. Zhou, L.R. Zheng and M. Wei, *Adv. Funct. Mater.*, 2020, **30**, 1907448.

[21] Z.H. Song, Q. Yin, S.H. Yang, Y.D. Miao, Y.J. Wu, Y.Z. Li, Y.J. Ren, Y.W. Sui, J.Q. Qi and J.B. Han, *Small*, 2023, **43**, 2302896.

[22] S.H. Yang, Q. Yin, Z.H. Song, F. Xu, Z.L. Xie, Y.J. Wu, S.L. Xu, Y.Z. Li, D.Y. Zhao, B. Xiao, X.L. Xue, J. Qi, Y.W. Sui and J.B. Han, *Mater. Horiz.*, 2023, **10**, 3429-3437.

[23] L.Z. Zhu, J.P. Ji, H.J. Yin and H.J. Zhao, *Energy Fuels*, 2023, **37**, 5607-5612.